RSC Advances

ROYAL SOCIETY OF CHEMISTRY

www.rsc.org/advances

Dip- and spin-assisted stereocomplexation-driven LbL self-assembly involving homochiral PVA-g-OLLA and PVA-g-ODLA copolymers

Mohamed Bahloul, Sébastien Pruvost, Etienne Fleury, Daniel Portinha,* and Aurélia Charlot*

Université de Lyon, F-69631, Lyon; INSA Lyon, F-69621,

UMR CNRS 5223, Ingénierie des Matériaux Polymères F-69621, Villeurbanne, France. Fax: +33 (0)4 72 43 85 27; Tel: +33 (0)4 72 43 63 38; E-mail: daniel.portinha@insa-lyon.fr, aurelia.charlot@insa-lyon.fr

Abstract

Layer by Layer (LbL) thin films stemming from the formation of stereocomplexes between oligolactate of opposite chirality (OLLA and ODLA) covalently anchored onto poly(vinyl alcohol) (PVA) chains is described herein for the first time. The feasibility to construct films by sequential adsorption of PVA-g-ODLA and PVA-g-OLLA graft copolymers is undertaken through the exploitation of two different film deposition techniques, namely dip- and spin-assisted processes. For both deposition methods, Infrared spectroscopy in ATR mode reveals a progressive accumulation of matter on the flat substrate during the successive cycle depositions and proves that co-crystallisation involving the two homochiral copolymers is the main driving force for the step by step film build up. Also, the effect of the deposition technique is assessed on the film features in terms of *i*) growth mechanism, *ii*) internal organization and *iii*) surface topology. The strong centrifugal forces associated with fast solvent elimination acting during spinning lead to thinner film with more uniform and homogeneous surface morphology in a much shorter time, than the ones resulting from the dip-assisted process. Such LbL nanometric films, induced by OLLA/ODLA interfacial stereocomplexation, open promising perspectives in the field of biodegradable self-assembled films.

Key words. poly(lactide), stereocomplex, dip-coating, spin-coating, multilayer films, layer by layer deposition, crystallisation-driven self-assembly

INTRODUCTION

The modification of inorganic surfaces by thin polymer films has been meeting a broad and profound interest in nanomaterial science. In this frame, the LbL self-assembly through the deposition of interacting polymers has emerged as a powerful bottom-up approach for the construction of films with precise control of thickness, architecture and composition at the nanoscale.[1,2] The interest is twofold: such thin self-assembled films and their formation mechanism are very relevant from fundamental[3-5] aspect together with a high potential to impart various functionalities to the substrate.[6-10] The very large majority of research dealing with LbL films has been devoted to the development of polyelectrolyte multilayers[11-14] and hydrogen bonds-mediated assemblies.[15-17] Nevertheless, the LbL assembly has successfully been extended to other attractive forces such as coordination bonds,[18] molecular recognition,[19] charge-transfer interactions,[20] host-guest interactions,[21] or stereocomplexation. Concerning this latter type of interaction, only very few examples have been reported in the literature. In this frame, the first category concerns polymers with precisely controlled tacticity, which are not so easy to synthesize. The examples deal with syndiotactic (st-) and isotactic (it-) derivatives, such as st-poly(methyl methacrylate) (PMMA) with it-PMMA,[22] it-PMMA combined to various st-poly(alkyl methacrylate)[23] and it-PMMA with poly(acid methacrylic).[24] The second category relies on the use of homochiral poly(lactide) (PLLA and PDLA, for levorotatory and dextrorotatory respectively). It is on this second particular class of stereocomplex that we have focused our investigation. Indeed, poly(lactide), which is a biobased and biodegradable polymer with an asymmetric carbon on each lactate repeating unit, can be found with different stereochemistry. While racemic PDLLA is amorphous, the optically pure isomers (PDLA and PLLA) are both crystallizable in an orthorhombic unit cell with a 10_3 helical conformation.[25] Interestingly, the equimolar mixture of PLLA and PDLA crystallizes in a trigonal unit cell, in which the left and right-handed 3_1 helices alternately

pack side by side through van der Waals interactions to form what is named stereocomplex.[25,26] Such mixtures display a melting point that is 50 °C above than the one of the enantiomeric precursors. Moreover, stereocomplexation is known to enhance mechanical performance, thermal stability and hydrolysis resistance. This is generally allocated to a more compact crystal structure.[27-28] As a consequence of these unique attributes, this type of stereocomplexation has also been exploited in sophisticated polymer architectures, such as di- or triblock copolymers [29-34] or graft copolymers[35,36] in view of generating objects in solvent medium with various morphologies (particles, micelles, cylinders)[29-34] or gels[37] induced by crystallisation. To the best of our knowledge, the only examples concerning the use of PLLA/PDLA stereocomplexation as driving force to build up LbL films were described by Akashi and co-workers, who nicely investigated the alternate deposition of PLLA and PDLA homopolymers.[38-40] The authors demonstrated the feasibility to prepare LbL films by dip-coating and they particularly showed that the sequential adsorption of PLA of opposite chirality yields heterogeneous and dotted morphology with high roughness. Also, they extended their work to the LbL deposition by inkjet printing.[41,42] By the way, Nakajima *et al.*, reported on the deposition of one layer of PLLA-containing di- and triblock (conjugated to poly(ethylene glycol)) onto PDLA chains pre-immobilized on a flat silicon surface.[43,44] They evidenced the formation of stereocomplexes on the surface, leading to bumpy surface structures but they focused their work on the deposition of only one copolymer layer, without constructing multilayers. To summarize, stereocomplexation-driven LbL assembled films including PLA-containing (co)polymers, such as graft copolymers have never been reported so far in literature.

In a previous paper, we described the synthesis of graft copolymers composed of poly(vinyl alcohol) (PVA) as main backbone bearing chiral oligolatacte (OLLA and ODLA) randomly distributed along the PVA chain. The copolymers were obtained through esterification

b)

ligation between PVA and narrowly dispersed acid chloride terminated OLA segments, and various PVA extent modifications (quantified by degree of substitution values in OLA grafts = DS_{Lac}) were declined.[45] Note that the degree of polymerization of OLA was optimized in view of favoring stereocomplexation.[46] We showed that, whatever the DS_{Lac} is, the mixture in DMSO at 40°C of PVA-g-OLLA with PVA-g-ODLA instantaneously turns turbid, as the result of the formation of crystallisation-driven interpolymer complexes (IPC).[45] Also, we emphasized that the stereocomplex formation - undertaken with a good solvent - is spontaneous and quasi-quantitative, which are motivating assets for the elaboration of thin films through the LbL approach.[47,48] In the continuous challenge to develop LbL films based on non-conventional physical interactions and with insight gained from our investigation in solution, we describe, for the first time, the use of chiral OLA-containing graft copolymers to construct films, in a LbL manner. We demonstrate that stereocomplexation-driven films can be engineered through either dip- or spin-assisted LbL assembly and we focus on the impact of the deposition process as it is well-established that it plays a key role on the resulting film features.[49-54] In particular, the growth mechanism, the internal structure of the layered interacting chains as well as the topography of the dip- and spin-deposited films are in-depth investigated.

RESULTS AND DISCUSSION

1. Film feasibility by dip- and spin-assisted LbL assembly

The general route towards the elaboration of [PVA-g-OLLA/PVA-g-ODLA]-based LbL films is represented in Fig. 1.

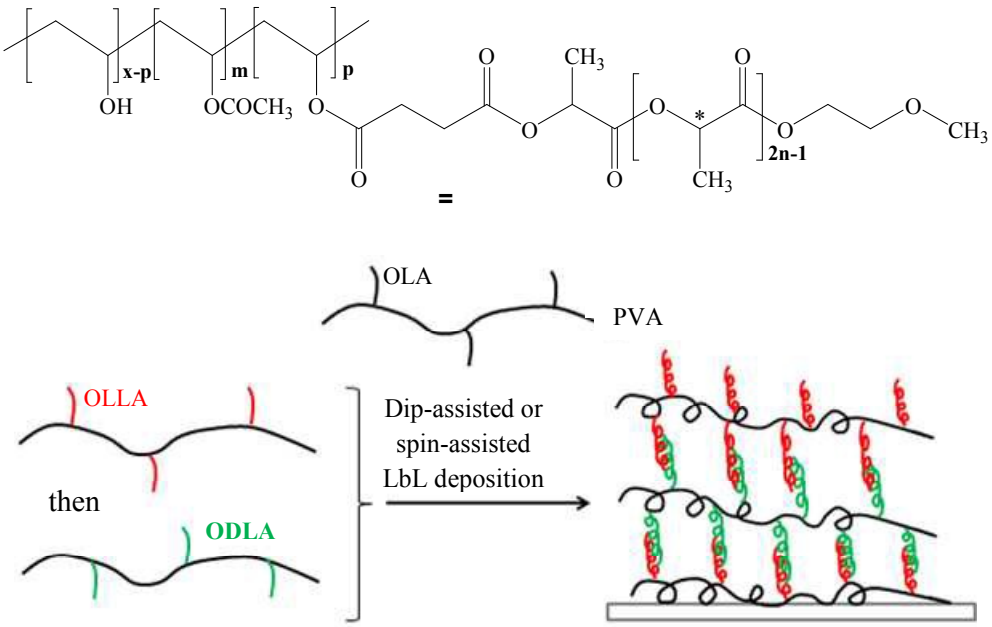

Fig. 1 Route to [PVA-g-OLLA/PVA-g-ODLA]-based LbL films.

Firstly, the sequential multilayer buildup was attempted by the conventional dipping method consisting in an alternate immersion of an activated wafer substrate in solutions of PVA-g-OLLA and PVA-g-ODLA ($C_{polymer}$ = 10 g/L) with DS_{Lac} of 8 % in DMSO at 40 °C for 15 minutes (see experimental part for more details). The use of DMSO combined to a temperature of 40°C were selected for the stepwise assembly as these conditions strongly favor the co-crystallization and the spontaneous stereocomplex formation.[45] The film after each deposited monolayer (PVA-g-OLLA and PVA-g-ODLA) up to 50 monolayers, was

analyzed by Infrared spectroscopy in ATR mode. The entire FTIR spectrum of the deposition of 50 monolayers (see Fig. SI1 and Table SI1) proves the presence of the PVA-g-OLA copolymers at the surface. Moreover, it is well established that FTIR spectroscopy is particularly adapted to prove the formation of stereocomplex between OLLA and ODLA.[36-38,55] Fig. 2 (A) shows a zoom of IR spectra on the 1600-1900 cm^{-1} range of the [PVA-g-OLLA/PVA-g-ODLA]$_{25}$ (50 monolayers) film (a), of the homochiral PVA-g-ODLA only (b) and of a racemic stereocomplex resulting from an equimolar mixture between PVA-g-OLLA and PVA-g-ODLA prepared by precipitation in ethanol (c).

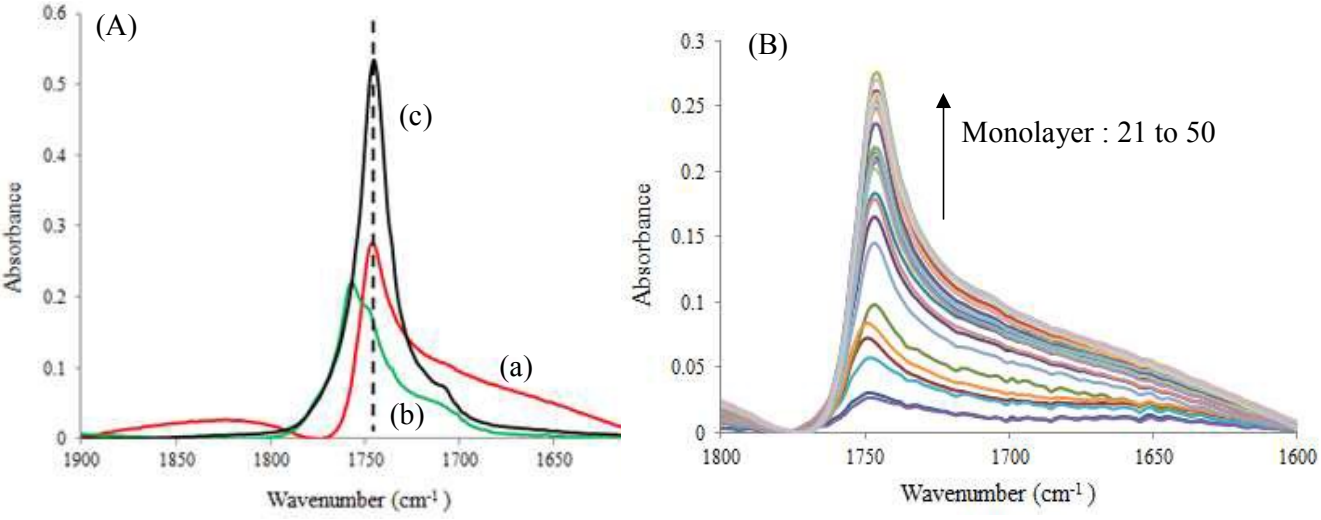

Fig. 2 (A) Magnification of ATR-FTIR spectrum on the carbonyl region of the [PVA-g-OLLA/PVA-g-ODLA]$_{25}$ after deposition by "dip-coating" of 50 monolayers (a), of pure PVA-g-ODLA only (b) and of a model (PVA-g-OLLA/PVA-g-ODLA) stereocomplex (c) and (B) Magnification of the evolution of the ATR-FTIR intensity of the C=O absorbance of the [PVA-g-OLLA/PVA-g-ODLA] film (DS_{Lac} = 8 %) after deposition by "dip-coating" from 21 up to 50 monolayers.

The IR response of the film exhibits the presence of only one absorption band at 1746 cm^{-1} (spectrum (a)), perfectly superimposed to the C=O signal belonging to the carbonyl functions involved into the stereocomplex cocrystal formed between the enantiomeric copolymers

(spectrum (c)). Moreover, the IR signal of C=0 from disordered DS_{Lac} units (visible at 1756 cm^{-1} in spectrum (b)) is not visible in the case of the film. Accordingly, we can state that $[PVA\text{-}g\text{-}OLLA/PVA\text{-}g\text{-}ODLA]_{25}$ film contains OLLA/ODLA stereocomplexes, without the concomitant presence of OLA homocrystals. A magnification of ATR-FTIR spectra of $[PVA\text{-}g\text{-}OLLA/PVA\text{-}g\text{-}ODLA]_n$ collected from 21 to 50 monolayers on the carbonyl zone is given in Fig. 2 (B). The intensity increase of the C=O absorption band with the number of deposited monolayers unambiguously proves the possibility to utilize the homochiral PVA-grafted copolymers to assemble multilayer thin films through successive immersion in a step by step manner. Note that the stereocomplexation-driven LbL assembly occurs from the deposition of 20 monolayers, as reflected by the existence of the unique C=0 absorbance signal at 1746 cm^{-1}. Thus, the LbL assembly process is mainly driven by the formation of stereocomplexes between OLLA and ODLA segments covalently anchored to PVA backbone. This completely supports our previous work, which has evidenced instantaneous, spontaneous and quasi quantitative stereocomplexation when PVA-g-OLLA and PVA-g-ODLA were mixed together in solvent medium.[45] However, we can reasonably think that it remains some unstereocomplexed carbonyl groups which cannot be detected by IR spectroscopy. The deposition of PVA-g-OLLA and PVA-g-ODLA with DS_{Lac} = 2 % was also performed. Unfortunately, we could not detect any IR signal up to a deposition of 50 monolayers, linked to the lack of sensitivity of this technique, which is probably due to a too low amount of polymers adsorbed on the silicon wafer (confirmed by wettability measurements, *vide-infra*). Thus, the extent of PVA modification by OLA grafts - quantified by the DS_{Lac} values - strongly impacts the deposition mechanism. It is reasonable to speculate that copolymers with DS_{Lac} = 2 % undergo lower interactions, related to a smaller number of OLA segments per PVA chain. Thus, we decided to exclusively focus the investigation on PVA-g-OLA with DS_{Lac} = 8 % in order to promote interactions/crystallisation between OLA segments.

Secondly, the multilayer film elaboration was attempted by successive spin-coating solution of PVA-g-OLLA and PVA-g-ODLA respectively dissolved at 2 g/L in DMSO (see experimental part). This deposition method has the advantage of being a fast fabrication process compared to the dip-assisted one. In this way, the film formation is induced not only by the interaction strength between the interacting entities but also by the strong air shear, centrifugal forces and fast solvent elimination occurring during the spinning rotation. Moreover, it is well established that the deposition process can affect the LbL deposition and the features of the as-obtained films, for instance in terms of internal structure,[49] growth mechanism and surface morphology[51] as well as thickness and roughness.[50] As for the films built-up by dip-coating, the substrate was analyzed by ATR-FTIR after each "spin-coated" PVA-g-OLLA or PVA-g-ODLA layer up to 50 monolayers. IR signal has been successfully detected from the monolayer 41 (Fig. SI 2) and as reflected by the C=O profile signal (Figure SI 3), it results that the multilayer construction is mainly mediated by the formation of stereocomplexes between PVA-g-OLLA and PVA-g-ODLA. Thus, it is possible to elaborate a $[PVA\text{-}g\text{-}OLLA/PVA\text{-}g\text{-}ODLA]_{25}$ multilayer LbL film in only 2 hours (*versus* 20 hours by dipping). The crystallisation-driven assembly between homochiral graft copolymers based on Van der Waals interactions between OLLA and ODLA segments is totally compatible with the spin-coating process.

The multilayer $[PVA\text{-}g\text{-}OLLA/PVA\text{-}g\text{-}ODLA]_{25}$ construction arising from both dip- and spin-coating was then monitored with increasing sequential monolayer deposition. The IR absorbance signal at 1746 cm^{-1} - assigned to C=O lactate groups involved in stereocomplex - was typically measured after the deposition of each monolayer (Fig. 3 (A) and (B)).

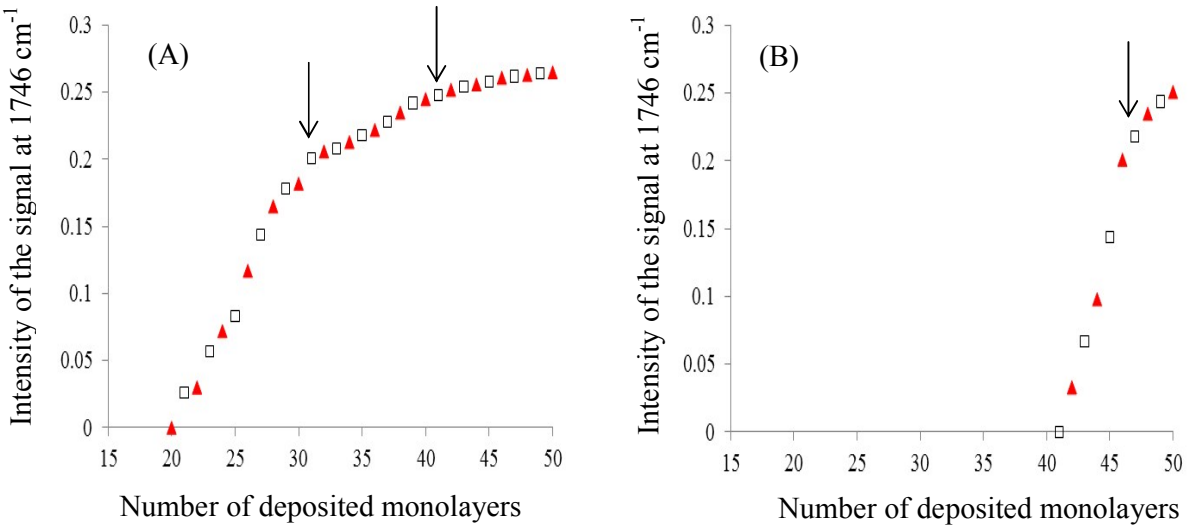

Fig. 3 Evolution of the IR intensity of the C=O absorbance at 1746 cm^{-1} of [PVA-g-OLLA/PVA-g-ODLA]$_n$ (DS_{Lac} = 8 %) multilayer films as a function of the number of monolayers deposited by (A) "dip-coating" and (B) by "spin-coating" process. (PVA-g-OLLA (▲) and PVA-g-ODLA (□)).

Firstly, the increase of the C=O absorbance intensity observed in Fig. 3 (A) and (B) underpins a global thickness evolution during the cycle deposition. Absorbance peaks for the spin-assisted LbL process have been detected from 41 deposited monolayers (Fig. 3 (B)) against 20 for the dip-mediated one (Fig. 3 (A)), much probably due to a much lower amount of deposited polymers. This was supported by the thickness of the resulting [PVA-g-OLLA/PVA-g-ODLA]$_{25}$ multilayered films (measured by atomic force microscopy after delicately performing a scratch on the surface, see Fig. SI 4), which is around 32 nm and 22 nm for the dip- and spin-deposited film, respectively. Note that these thicknesses obtained for 25 deposited bilayers are particularly low, compared to systems developing electrostatic interactions[56] or hydrogen bonds,[57] much probably related to the nature of the interaction between the homochiral PVA-g-OLA, based on a compact packing of β-form 3_1 helices. Furthermore, the statement that dipping leads to thicker films as compared to spin-coated ones, has been reported in literature, in particular for multilayers composed of weakly bound

polyelectrolytes.[51,53] For instance, Hong *et al.* were interested on the impact of deposition technique on weak ionic interactions-mediated assemblies and measured a thickness of 412 nm for a [PS-b-P4VP/PS-b-PAA]$_{30}$ film constructed by dip against 59.5 nm for a film elaborated by spin.[51] In our case, the fast elimination of solvent during the spinning step facilitates Van der Waals attractive interactions between PVA-g-OLLA and PVA-g-ODLA and minimizes adsorption of more outlying copolymers, resulting in a lower amount of deposited polymer. Also, the strong air shear and centrifugal forces are so dominant as they displace more weakly adsorbed PVA-g-OLA chains. Conversely, dip-assisted method allows enough time for PVA-g-OLA chains to diffuse and to adsorb onto the substrate *via* stereocomplexation. Moreover, the dip-mediated construction exhibits a growth mechanism in three steps that are each linear (Fig. 3 (A)). The linearity in each regime indicates that the monolayer amount deposited at each deposition cycle is constant. The slope divergences observed at the 30th and 40th layer can be attributed to a peculiar chain organization between the two partners, which seems to be dependent on the number of deposited monolayers. Also, this break in slope might be explained by a surface coverage and by an interpenetration degree of deposited polymers which changes all along the deposition cycle. The polymer deposition can induce a roughness variation, which might change the apparent surface area for polymer deposition. By the way, possible partial desorption during the rinsing steps can explain the third absorbance evolution characterized by the lowest slope. Fig. 3 (B) indicates that the spin-mediated film construction follows a two-step growth mechanism characterized by two linear evolutions with a slope divergence at the 45th deposited monolayer. This differs from more conventional LbL films mediated by electrostatic or hydrogen interactions,[6,58,59] for which the growth mechanism often follows only one regime (linear or exponential). Herein, we can reasonably attribute these observations to the not so-common driving force for the construction of the LbL films, relied on Van der Waals-mediated crystallization. In any case,

whatever the deposition technique is, the IR profiles evidence that after the deposition of one PVA-g-OLLA layer (layer (*i*)), one part of OLLA immobilized onto PVA backbone forms stereocomplexes with ODLA segments belonging to the PVA-g-ODLA sublayer (layer (*i-1*)) while one other part of OLLA remains available to efficiently interact with the next deposited layer (layer (*i+1*)).

2. Internal structure and topology features of the resulting films

The surface wettability measured by the water contact angle values (θ_{water}) reflects the first 5-10 Å of the film's outermost surface and is not only sensitive to the chemical composition but also to the surface topology and in the case of LbL films, to the degree of interdigitation between the adsorbed polymers.[60] The θ_{water} values of pristine PVA, homochiral PVA-g-ODLA, and PVA-g-OLLA as well as PVA-g-ODLA/PVA-g-OLLA stereocomplex independently prepared are provided in Table 1.

Sample	θ_{water} value (°)
PVA*	11.5 ± 1.2
PVA-g-ODLA (DS_{Lac} = 8 %)*	33.7 ± 3.7
PVA-g-OLLA (DS_{Lac} = 8 %)*	26.1 ± 2.9
SC of PVA-g-OLDA/PVA-g-OLLA (DS_{Lac} = 8 %)**	55.5 ± 3.6

Table 1 Values of water contact angle for various samples * *Solutions deposited by "spin-coating" (C = 10 g/L) on a silicon wafer ** Solid pellet processed from stereocomplex prepared by precipitation in ethanol*

A close inspection of Table 1 shows that the θ_{water} values of PVA-g-OL(D)LA are higher than the one of pure PVA, related to the more hydrophobic character of OLA segments tethered to

PVA backbone and mostly located at the air interface. Note that the θ_{water} of PVA-g-ODLA is superior to the one of PVA-g-OLLA (33.7 ° *versus* 26.1 °, respectively). Given the similar chemical structure of these two copolymers, the θ_{water} difference might arise from a different interfacial OLA conformation, governed by the chirality (L or D) that leads to a change of both local surface chemical composition and roughness. Such a θ_{water} difference as a function of the stereochemistry of PLA and a higher value for the D-enantiomer support works of Serizawa *et al.*, who measured θ_{water} values of 61 ° and 69 ° for PLLA and PDLA homopolymers, respectively.[38] Note that a conformation-induced θ_{water} difference was also reported for it- and st-PMMA.[22] The water contact angle determined on PVA-g-OLLA/PVA-g-ODLA stereocomplex independently prepared is higher (55 °), linked to a peculiar spatial rearrangement of the copolymers under co-crystallised form. Such a θ_{water} increase between the homochiral polymers and the related stereocomplex was highlighted in the case of PLLA and PDLA homopolymer.[38] Given that the θ_{water} is strongly dependent on the OLA segments conformation, the values in Table 1 are just provided as guidelines. Indeed, the θ_{water} value for PVA-g-OLLA/PVA-g-ODLA stereocomplex corresponds to the deposition of only one layer composed of preformed stereocomplexes, while our work consist in a sequential and successive deposition of each enantiomeric copolymer on the substrate.

Figure 4 depicts the θ_{water} value evolution of the dip- and spin-constructed [PVA-g-OLLA/PVA-g-ODLA]$_n$ films, measured after each deposited monolayer. The investigation of the wettability during the film deposition was shown to be particularly well-suited to gain insight on the internal structure of H-bond-mediated films,[15] polyelectrolyte multilayers [61] and also films based on it- and st-PMMA.[22]

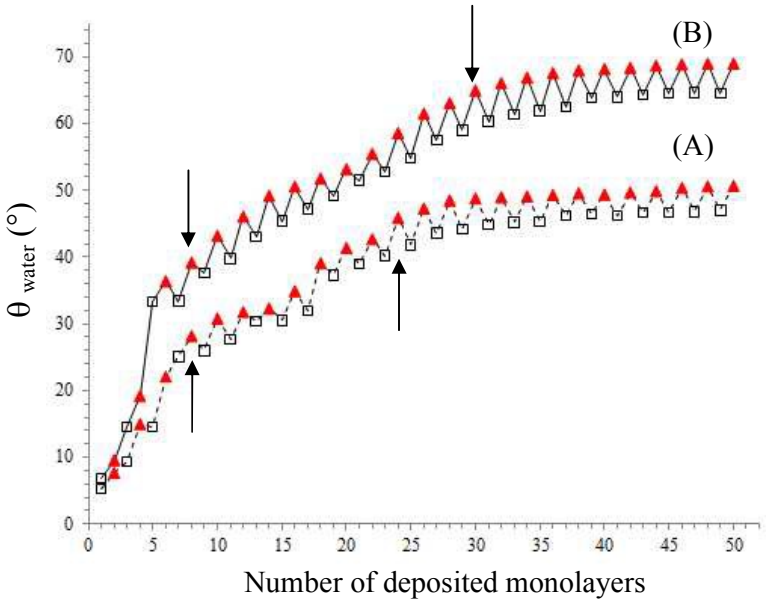

Fig. 4 Evolution of θ_{water} of $[PVA\text{-}g\text{-}OLLA/PVA\text{-}g\text{-}ODLA]_n$ (DS_{Lac} = 8 %) multilayer films as a function of the number of monolayers deposited by (A) "dip-coating" and (B) "spin-coating" processes (PVA-g-OLLA (▲) and PVA-g-ODLA (□)).

Whatever the deposition method employed to construct $[PVA\text{-}g\text{-}OLLA/PVA\text{-}g\text{-}ODLA]_n$ LbL film is, the θ_{water} evolution follows rather similar profiles. As can be seen in Figure 4 (A and B), the change of water contact angle can be divided in three domains (indicated by arrows): *i*) a continuous θ_{water} increase without alternate variation up to 10 monolayers, *ii*) the second laying from 10 to 25 or 30 layers where the θ_{water} stochastically changes as a function of the deposited polymer (with θ_{water} of PVA-g-ODLA superior to the one of PVA-g-OLLA, as reported in Table 1), and *iii*) the last domain with a distinct periodic oscillation when the top surface layer is alternatively varied. Note that from the first deposited monolayer, a water contact angle change is observed (for both deposition methods), while no IR signal was observed before the 20^{th} and the 41^{th} deposited layer for the dip- and spin-assisted films, respectively. Thus, we can ascertain that the lack of IR detection was solely due to a too limited amount of copolymers.

The first domain could be seen as an induction period, where the initial assembly yields a weak and scattered deposition and thus is strongly influenced by the underlying Si-wafer substrate, as established in literature.[15,62] In the second domain, the increase of the difference in θ_{water} between the two homochiral PVA-g-OLA can be ascribed to the continuous surface coverage occurring all along the deposition cycle. In the third domain, the same θ_{water} value recorded after the deposition of one given enantiomeric polymer demonstrates that the extreme surface features (chemical composition and chain conformations) do not change. Note again that it remains delicate to compare the θ_{water} collected after the deposition of one given copolymer with values reported for homochiral polymers in Table 1, since the water wettability is closely dependent on the OLA grafts density present at the surface as well as their spatial rearrangement. Also, it is possible that the film is not perfectly well-compartmentalized and individualized but rather stratified. The θ_{water} value can reflect the mixed nature of a layer due to a partial diffusion of one given PVA-OLA layer (*i*) into the sublayers (*i-1*, *i-2*, *i-3*…) and even the migration of PVA-g-OLA underlayers up to the outermost layer, which both might happen during the successive immersion steps. Note that the same trend was found for films constructed from PVA-g-OLA with DS_{Lac} = 2 % deposited by dip-coating (Figure SI 5). Although the two wettability evolution profiles are relatively similar, the water contact values recorded onto spin-assisted films are quite higher (Figure 4 (B)), which can be the consequence of differences in surface chemical composition and topology (see AFM analysis) stemmed from the deposition process. Indeed, as previously mentioned, the high speed spin-deposition induces strong air shear and centrifugal forces impacting the polymer adsorption mechanism.

Fig. 5 (A) and (B) compare the topographic images of $[PVA\text{-}g\text{-}OLLA/PVA\text{-}g\text{-}ODLA]_{25}$ (DS_{Lac} = 8 %), using the two LbL assembly methods (dip and spin, respectively) by atomic force microscopy in tapping mode. First, the presence of organic matter observed in AFM

images, compared with AFM analysis of neat silicon wafer exhibiting a Rq value of 0.496 nm (Figure SI 6) enables to ascertain that the stereocomplexation-driven LbL assembly based on the alternate deposition of 50 layers of homochiral PVA-g-OLA leads to a covering multilayer films. Also, the collections on 2 μm × 2 μm indicate different surface morphologies of the two multilayer films (Fig. 5 (a) and (d)).

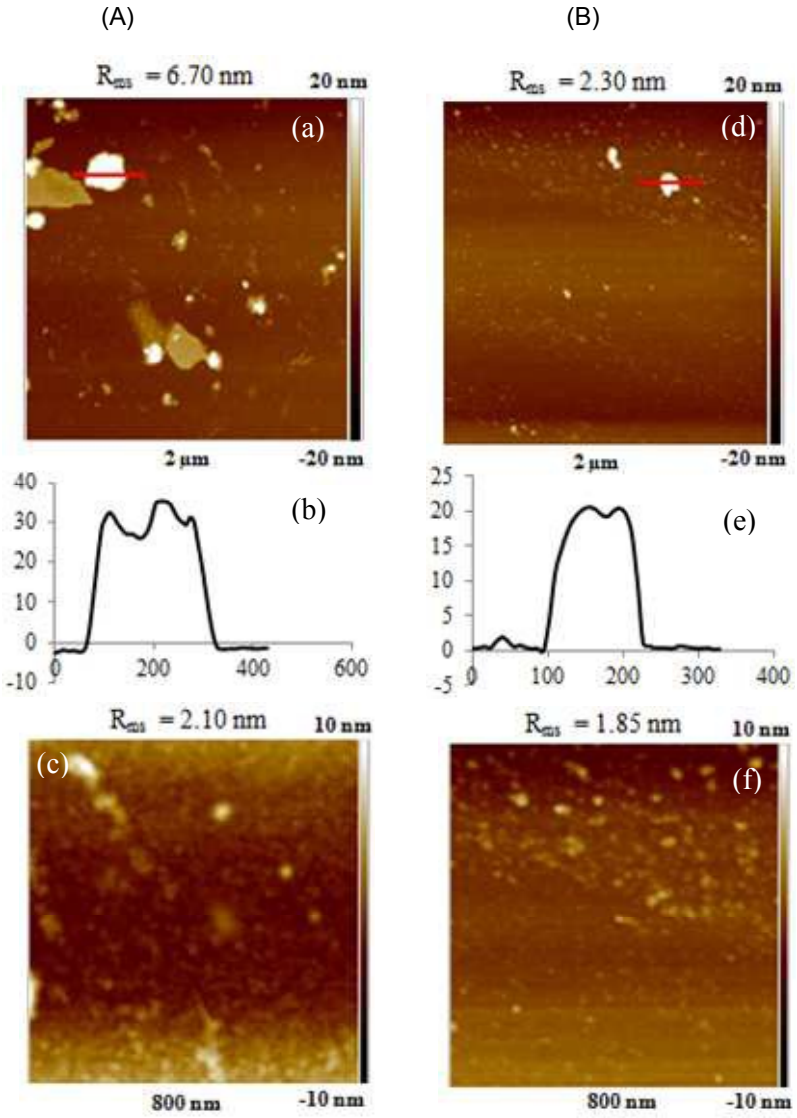

Fig. 5 AFM topologic images of [PVA-g-OLLA/PVA-g-ODLA]$_{25}$ (50 monolayers, DS_{Lac} = 8%) deposited by (A) "dip-coating" (a,c) and by (B)"spin-coating" (d,f) collected on different scales with the corresponding height profiles (b and e).

The dip-conducted [PVA-g-OLLA/PVA-g-ODLA]$_{25}$ surface morphology is characterized by the presence of several scattered polymorphic and polydisperse polymer aggregates which are stochastically dispersed on the surface and which can reach 200 nm in lateral dimension and almost 36 nm in height (Fig. 5 (a) and (b)). The presence of some coacervates induces high R_q value (6.70 nm). These large diameters are probably overestimated due to the effect of the

AFM tip. The surface aggregates are constituted of multiple stereocomplexed PVA-g-OLA copolymers, which yield segregated surface zones. Moreover, it is important to keep in mind that the topology can be affected by the drying step which can lead to an additional surface layer collapse. The magnification onto a zone of 800 nm × 800 nm exhibits a more homogeneous granular texture, characterized by a lower R_q value of 2.10 nm. This morphology differs from the ones reported for PLLA deposition onto a PDLA-immobilized surface which yielded bumpy surface.[43,44] Moreover, dip-assisted [PLLA/PDLA] LbL films prepared by Akashi *et al.* showed nodular topology with very high R_{ms} (up to 14.5 nm for only 12 deposited bilayers) ascribed to the fact that one chiral PLA is surrounded by three of its enantiomer in the trigonal crystal system of the stereocomplex.[38] In our case, grafted copolymers and not homopolymers are employed, which closely impacts the modes of chain adsorption and thus the final observed morphology. By contrast, AFM pictures of the spin-assembled $[PVA\text{-}g\text{-}OLLA/PVA\text{-}g\text{-}ODLA]_{25}$ (Fig. 5 (d)) film exhibit more uniform and homogeneous morphology with only scarce aggregates with smallest dimension (up to 20 nm in height and 100 nm in lateral dimension, Fig. 5 (e)), as also reflected by a lower R_q value (2.30 nm). The zoom on a zone of 800 nm × 800 nm underpins a rather featureless surface morphology (Fig. 5 (f)). Thus, spin-assembled films appear smoother and flatter, which is consistent with reported bibliography.[50,51] This can be rationalized by considering the short period of spinning and the strong centrifugal forces, which quite limits polymer arrangement onto the surface and leads to packed and ordered structures with reduced internal interfacial mixing, in contrast with the adsorption mechanism during dip-assisted deposition which is mainly diffusion-controlled. The shear stress successfully competes with intermolecular binding, resulting in chain flattening. As compared to drying step under nitrogen flux applied in dipping technique, the very high speed of rotation arising from spinning deposition enhances the evaporation of most of solvent (DMSO), which is a key factor controlling the

conformation of adsorbed polymers and film structure. Moreover, it has been shown that as a function of the nature and the strength of the driving force, spin-assisted LbL assembly leads to highly stratified films, in comparison with more intermixed layers stemming from dip-assisted ones. It is the case for instance for polyelectrolyte multilayers made of weakly bound polyanions and polycations.[52,54] This can also explain the differences in water contact angle values between the [PVA-g-OLLA/PVA-g-ODLA] films assembled by dip- or spin-coating.

As OLLA/ODLA based-stereocomplex results in crystalline domains with high melting temperature around 205 °C, it is reasonable to speculate that a heat treatment followed by a cooling-down step might induce a chain reorganization within films. Thus, the [PVA-g-OLLA/PVA-g-ODLA]$_{25}$ dip-assisted film was subjected to high temperature (220 °C) under vacuum for 15 minutes, followed by a cooling-down up to room temperature. AFM analysis revealed noticeable change morphology stemmed from the thermal cycle (Fig. SI 7). Large triangular shape aggregates spatially extended on more than 1 μm are visualized. The heat thermal treatment can play on both size and morphology of crystals and also on the crystallinity rate. This triangle-based geometry, not so common since it is related to no crystalline cell, has already been reported by Brizzolara *et al.*,[63] Okihara *et al.*,[64] and by Cartier and co-workers for PLLA/PDLA blends.[65] In particular, Cartier *et al.* ascribed this morphology to differences in crystallization rate of the PLLA and PDLA sequences, which can occur for imperfect mixtures (blends of enantiomeric polymers with different molecular weights and/or different dispersity index, or non equimolar blends).[65] In our case, the OLA grafts have quite similar DP_n and dispersity index (see experimental part). The blends were prepared with respect of stoichiometric conditions, but by considering the uncertainties of NMR measurements (around 5%), which allowed us for determining the DP_{lac} and the DS_{Lac}, it is reasonable to do the assumption that the blend contains a slight excess of one enantiomeric OLA. Moreover, graft copolymers (and not homopolymers) are used in our

work, contrary to most of reported works. The presence of PVA backbone might constrain the growth crystal along specific directions, which can explain the observed morphology. Furthers works are in progress to gain insights on this peculiar aspect.

Conclusions

In summation, we emphasized the feasibility of constructing novel stereocomplexation-driven LbL films involving homochiral PVA-g-OLLA and PVA-g-ODLA graft copolymers, synthesized by a "grafting onto" strategy between PVA backbone and acid chloride-terminated narrowly dispersed oligolactate derivatives. Additionally, we demonstrated that [PVA-g-OLLA/PVA-g-ODLA] films can be obtained by different deposition process techniques, such as dip- and spin-coating. We clearly showed that the formation of stereocomplexes between the enantiomeric graft copolymers is the main driving force for the construction of the LbL films. The nature of the non-covalent interactions (Van der Waals forces) and, in particular the compactness of the crystalline structure of stereocomplexes arising from optically pure OLA segments, leads to films that are thinner than the more conventional ones mediated by electrostatic interactions or hydrogen bonds. Also, the deposition technique impacts the resulting features films, notably in terms of thickness and surface topology. Both the strong shear forces and the fast elimination of the solvent occurring during the spinning step, yields thinner and more uniform/homogeneous films induced by a peculiar chain conformation adopted by adsorbed copolymers. The wettability measurements revealed that from a threshold number of deposited monolayers, the films are well stratified. The approach described herein opens new perspectives for the design and the exploitation of nanometric films based through well-defined and degradable interacting groups.

Materials and Methods

Silicon wafers were purchased from Sil'tronix. They were cut into appropriate dimensions (typically 1 cm × 1 cm) before use, and activated by ozonolysis for 30 min prior to any deposition of polymers. Anhydrous dimethylsulfoxide (99.9 %) was obtained from Aldrich and was used without prior purification. Partially acetylated PVA (Mn ~ 126 000 g/mol, degree of substitution in acetate groups, DS_{Ac} = (5.1 ± 0.2) %) purchased from Aldrich was used. The synthesis and the molecular characterization of OLLA (DP_{Lac} = 20, Đ = 1.26), PVA-g-OLLA, ODLA (DP_{Lac} = 21, Đ = 1.28) and PVA-g-ODLA were presented in detail in a previous work.[45] Note that intensive washing steps with selective solvents (toluene/THF) have been applied in order to efficiently eliminate ungrafted OLA species.[45] Different degrees of substitution in oligolactate oligomers (DS_{Lac} = 2.5 % ± 0.2 and 8.0 % ± 0.4) were targeted and used in this work.[45] The degree of substitution in oligolactate corresponds to the number of OLA segments for one hundred PVA repeating units. In the following of this article, the used graft copolymer will be identified as PVA-g-O*X*LA (DS_{Lac} = 2 or 8 %) where *X* = L or D. PVA-g-OLA solutions were prepared through a dissolution step in DMSO at 40 °C for 16 h, whatever the structure (DS_{Lac}, chirality) and concentration were.

For the preparation of the model PVA-g-OLLA/PVA-g-ODLA stereocomplex under powder form, around 200 mg of PVA-g-OLLA and 200 mg of PVA-g-ODLA (both with DS_{Lac} = 8 %) were separately solubilized in 20 mL of anhydrous DMSO at 40 °C overnight, then mixed under stirring. The blend was isolated by precipitation in ethanol, filtrated and then dried under vacuum at 80 °C for 24 h.

Preparation of Multilayer Films

In a typical layer by layer deposition procedure by "dip-coating", an activated silicon wafer was first immersed in a DMSO solution of PVA-g-OLLA (DS_{Lac} = 8 % or 2 %, and C = 10

g/L) for 15 min at 40 °C, rinsed twice in two different bathes of DMSO (dynamically for 2 min and statically for 5 min) and then dried with nitrogen stream. The silicon wafer was then dipped in DMSO solution of PVA-g-ODLA (same DS_{Lac} and concentration) for 15 min at 40°C, rinsed and dried by following the same procedure. A bilayer (n) is constituted of one [PVA-g-OLLA/PVA-g-ODLA] combination. This cycle was then repeated as necessary to obtain a multilayer film composed of n = 25 bilayers, *i.e.* 50 monolayers. The resulting dip-assisted film was heat-treated in a vacuum oven at 220°C for 15 min, followed by a cooling-down at room temperature.

In the case of the spin-assisted LbL method, around 100 µL of a PVA-g-OLLA solution (C = 2 g/L) was deposited onto the activated silicon substrate, which was then spun for 30 s at a speed of 3000 rpm using a Polo Spin 150i / 200i spin-coater type from SPS-Europe. After the deposition of one monolayer, the substrate was rinsed with pure DMSO by using the same spinning time and speed, and dried by a gentle stream of nitrogen gas. PVA-g-ODLA was then deposited by following the same protocol and the cycle was repeated to produce 50 monolayers.

Instrumentation Methods

Attenuated total reflection Fourier transform infrared (ATR-FTIR) spectra were recorded using a Nicolet iS10 apparatus (diamond crystal) with a resolution of 2 cm^{-1} and a 256 scan accumulation. Water contact angle (θ_{water}) measurements were carried out using a GBX Digidrop contact angle meter equipped with a CDD2/3″ camera with the sessile drop method and by using Milli-Q quality water as probe liquid. The tabulated results are the average of at least six measurements on different parts of each sample. AFM (atomic force microscope) images were acquired in intermittent contact mode (tapping mode), on a wafer of 1 cm × 1 cm, in air at room temperature using a AFM Bruker Multimode 8 equipped with Nanoscope V controller. The scanning speed for image acquisition is 0.5 Hz. The used tips are TAP 150

with a radius of curvature of 8 nm. The surface roughness R_q was obtained by processing images using the Nanoscope Analysis software (version 1.5). In order to access to the film thickness, an indentation was delicately performed with a razor blade by ensuring a good access to the silicon substrate and the elimination of the removed polymer from the surface. The height difference created by the indentation can be probed by AFM topology, which provides the thickness deposition.

Acknowledgements

The authors thank the French Ministry of Research for M. B.'s Ph.D. grant.

Notes and references:

1 K. Ariga, Y. Yamauchi, G. Rydzek, Q. Ji, Y. Yonamine, K. C-W. Wu and J. P. Hill, *Chem. Lett.*, 2014, **43**, 36-68.
2 J. Borges and J-F. Mano, *Chem. Rev.*, 2014, **114**, 8883-8942.
3 P. Laurent, G. Souharce, J. Duchet-Rum
eau, D. Portinha and A. Charlot, *Soft Matter*, 2012, **8**, 715–725.
4 S. Owusu-Nkwantabisah, M. Gammana and P. Carl, *Langmuir*, 2014, **30**, 11696–11703.
5 M. L. Ohnsorg, C. K. Beaudoin and M. E. Anderson, *Langmuir*, 2015, **31**, 6114–6121.
6 A. Charlot, V. Sciannaméa, S. Lenoir, E. Faure, R. Jérôme, C. Jérôme, C. Van De Weerdt, J. Martial, C. Archambeau, N. Willet, A.-S. Duwez, C.-A. Fustin and C. Detrembleur, *J. Mater. Chem*., 2009, **19**, 4117–4125.
7 Y. Liu, J. Li, X. Cheng, X. Ren and T. S. Huang, *J. Mater. Chem. B*, 2015, **3**, 1446–1454.
8 Y. Choi, S. Choi, H. Young, J. M. Liu, B.-S. Kim and G. Kim, *ACS Appl. Mater. Interfaces*, 2014, **6**, 17352–17357.
9 C. Aulin, E. Karabulut, A. Tran, L. Wågberg and T. Lindström, *ACS Appl. Mater. Interfaces*, 2013, **5**, 7352–7359.
10 M. D. Miller and M. L. Bruening, *Langmuir*, 2004, **20**, 11545–11551.
11 G. Decher, *Science*, 1997, **277**, 1232–1237.
12 T. Alonso, J. Irigoyen, J. J. Iturri, I. L. Larena and S. E. Moya, *Soft Matter*, 2013, **9**, 1920–1928.
13 J. B. Schlenoff, *Langmuir*, 2009, ***25***, 14007–14010.
14 R. Zahn, J. Vörös and T. Zambelli, *Langmuir*, 2014, ***30***, 12057–12066.
15 J. Chen, J. Duchet, D. Portinha and A. Charlot, *Langmuir*, 2014, **35**, 10740–10750.
16 Y. Takemoto, H. Ajiro and M. Akashi, *Langmuir*, 2015, ***31***, 6863–6869.
17 I. Erel, H. E. Karahan, C. Tuncer, V. Bütün and A. L. Demirel, *Soft Matter*, 2012, **8**, 827–836.
18 H. Lee, L. J. Kepley, H.-G. Hong and T. E. Mallouk, *J. Am. Chem. Soc*., 1988, **110**, 618–620.

19 W. Müller, H. Ringsdorf, E. Rump, G. Wildburg, X. Zhang, L. Angermaier, W. Knoll, M. Liley and J. Spinke, *Science*, 1993, **262**, 1706–1708.
20 X. Wang, K. Naka, H. Itoh, T. Uemura and Y. Chujo, *Macromolecules*, 2003, **36**, 533–535.
21 O. Crespo-Biel, B. Dordi, D. N. Reinhoudt and J. Huskens, *J. Am. Chem. Soc.*, 2005, **127**, 7594–7600.
22 T. Serizawa, K.-I. Hamada, T. Kitayama, N. Fujimoto, K. Hatada and M. Akashi, *J. Am. Chem. Soc.*, 2000, **122**, 1891–1899.
23 T. Kitayama, N. Fujimoto, Y. Terawaki and K. Hatada, *Polym. Bull.*, 1990, **23**, 279–286.
24 T. Kida, M. Mouri, K. Kondo and M. Akashi, *Langmuir*, 2012, **28**, 15378–15384.
25 Y. Ikada, K. Jamshidi, H. Tsuji and S.-H. Hyon, *Macromolecules*, 1987, **20**, 904–906.
26 H. Tsuji, *Macromol. Biosci.*, 2005, **5**, 569−597.
27 K. Fukushima and Y. Kimura, *Polym. Int.*, 2006, **55**, 626−642.
28 L. Yu, K. Dean and L. Li, *Prog. Polym. Sci.*, 2006, **31**, 576−602.
29 Z. Zhao, Z. Zhang, L. Chen, Y. Cao, C. He and X. Chen, *Langmuir*, 2013, **29**, 13072–13080.
30 L. Sun, A. Pitto-Bary, N. Kirby, T. L. Schiller, A. M. Sanchez, M. A. Dyson, J. Sloan, N. R. Wilson, R. K. O'Reilly and A. P. Dove, *Nature Commun.*, 2014, **5:5746**, 1–*9*.
31 Z. Li, D. Yuan, X. Fan, B. H. Tan and C. He, *Langmuir, 2015,* **31***,* 2321–2333.
32 D. Portinha, J. Belleney, L. Bouteiller, S. Pensec, N. Spassky and C. Chassenieux, *Macromolecules*, 2002, **35**, 1484–*1486.*
33 D. Portinha, F. Boué, L. Bouteiller, G. Carrot, C. Chassenieux, S. Pensec and G. Reiter, *Macromolecules*, 2007, **40**, 4037–4042.
34 D. Portinha, L. Bouteiller, S. Pensec, A. Richez and C. Chassenieux, *Macromolecules*, 2004, **37**, 3401–3406.
35 D. W. Lim, S. H. Choi and T. G. A. Park, *Macromol. Rapid Comm.*, 2000, **21**, 464–471.
36 S. J. de Jong, S. C. de Smedt, M. W. C. Wahls, J. Demeester, J. J. Kettenes-van den Bosch and W. E. Hennink, *Macromolecules*, 2000, **33**, 3680–3686.
37 S. J. de Jong, C. F. van Nostrum, L. M. J. Kroon-Batenburg, J. J. Kettenes-van den Bosch and W. E. Hennink, *J. App. Polym. Sci.*, 2002, **86**, 289–293.
38 T. Serizawa, H. Yamashita, T. Fujiwara, Y. Kimura and M. Akashi, *Macromolecules*, 2001, **34**, 1996–2001.
39 T. Serizawa, Y. Arikawa, K.-I. Hamada, H. Yamashita, T. Fujiwara, Y. Kimura and M. Akashi, *Macromolecules*, 2003, **36**, 1762–1765.
40 M. Matsusaki, H. Ajiro, T. Kida, Y. Serizawa and M. Akashi, *Adv. Mater.*, 2012, **24**, 454–474.
41 T. Akagi, T. Fujiwara and M. Akashi, *Angew. Chem. Int. Ed.*, 2012, **51**, 5493–5496.
42 T. Akagi, T. Fujiwara and M. Akashi, *Langmuir*, 2014, **30**, 1669–1976.
43 H. Nakajima, M. Nakajima, T. Fujiwara, C. W. Lee, T. Aoki and Y. Kimura, *Macromolecules*, 2012, **45**, 5993–6001.
44 M. Nakajima, H. Nakajima, T. Fujiwara, Y. Kimura and S. Sasaki, *Langmuir*, 2014, **30**, 14030–14038.
45 M. Bahloul, C. Chamignon, S. Pruvost, E. Fleury, A. Charlot and D. Portinha, Accepted in *Polymer* 2015.
46 S. J. de Jong, W. N. E. Van Dijk-Wolthuis, J. J. Kettenes-van den Bosch, P. J. W. Schuyl and W. E. Hennink, *Macromolecules*, 1998, **31**, 6397–6402.
47 J. Chen, L. Dumas, J. Duchet-Rumeau, E. Fleury, A. Charlot and D. Portinha, *J. Polym. Sci., Part A: Polym. Chem.*, 2012, **50**, 3452–3460.
48 J. Chen, D. Vuluga, B. Crousse, J. Legros, J. Duchet-Rumeau, A. Charlot and D. Portinha, *Polymer*, 2013, **54**, 3757–3766.

49 C. Sung, K. Hearn, D. K. Reid, A. Vidyasagar and J. L. Lutkenhaus, *Langmuir*, 2013, **29**, 8907–8913.
50 J. Seo, J. L. Lutkenhaus, J. Kim, P. T. Hammond and K. Char, *Langmuir*, 2008, **24**, 7995–8000.
51 J. Hong and H. Park, *Colloids and Surfaces A : Physicochem. Eng. Aspects*, 2011, **381**, 7–12.
52 E. Kharlampieva, V. Kozlovskaya, J. Chan, J. F. Ankner and V. V. Tsukruk, *Langmuir*, 2009, ***25***, 14017–14024.
53 A. Zhuk, V. Selin, I. Zhuk, B. Belov, J. F. Ankner and S. A. Sukhishvili, *Langmuir*, 2015, **31**, 3889–3896.
54 Y. M. Lee, D. K. Park, W.-S. Choe, S. M. Cho, G. Y. Han, J. Park and P. J. Yoo, *J. Nanoscience and Nanotechnology*, 2009, **9**, 7467–7472.
55 D. W. Lim and T. G. Park, *J. Appl. Polym. Sci.*, 2000, **75**, 1615–1623.
56 C. de Saint-Aubin, J. Hemmerlé, F. Boulmedais, M.-F. Vallat, M. Nardin and P. Schaaf, *Langmuir*, 2012, **28**, 8681–8691.
57 B.-S. Kim, S. W. Park and P. T. Hammond, *ACS Nano*, 2008, **2**, 386–392.
58 H. Zhang, Z. Wang, Y. Zhang and X. Zhang, *Langmuir*, 2004, **20**, 9366–9370.
59 P. Podsiadlo, M. Michel, J. Lee, E. Verploegen, N. W. S. Kam, V. Ball, J. Lee, Y. Qi, A. J. Hart, P. T. Hammond and N. A. Kotov, *Nano Lett.*, 2008, ***8***, 1762–1770.
60 A. Quinn, E. Tjipto, A. Yu, T. R. Gengenbach and F. Caruso, *Langmuir*, 2007, **23**, 4944–4949.
61 M. An and J.-D. Hong, *Colloids surf A : Physiochem. Eng. Aspects*, 2009, **348**, 301–304.
62 J. Bico, C. Tordeux and D. Quéré, *Europhys. Lett.*, 2001, **55**, 214–220.
63 D. Brizzolara, H.-J. Cantow, K. Diederichs, E. Keller and A. J. Domb, *Macromolecules*, 1996, **29**, 191–197.
64 T. Okihara, M. Tsuji, A. Kawaguchi, K.-I. Katayama, H. Tsuji, S.-H. Hyon and Y. Ikada, *J. Macromol. Sci. Phys.*, 1991, **B30 (1&2)**, 119–140.
65 L. Cartier, T. Okihara and B. Lotz, *Macromolecules*, 1997, **30**, 6313–6322.

Table of Contents Entry

Dip- and spin-assisted stereocomplexation-driven LbL self-assembly involving homochiral PVA-g-OLLA and PVA-g-ODLA copolymers

Mohamed Bahloul, Sébastien Pruvost, Etienne Fleury, Daniel Portinha,* and Aurélia Charlot*

Université de Lyon, F-69631, Lyon; INSA Lyon, F-69621, UMR CNRS 5223, Ingénierie des Matériaux Polymères F-69621, Villeurbanne, France. Fax: +33 (0)4 72 43 85 27; Tel: +33 (0)4 72 43 63 38; E-mail: daniel.portinha@insa-lyon.fr, aurelia.charlot@insa-lyon.fr